Enhancing Speckle Statistics for Imaging Inside Scattering Media

Supplementary Appendix

A. ANALYZING CORRELATION PROPERTIES IN LSI MEASUREMENTS

In this section, we formulate and prove a few properties of LSI modulations mentioned in the main paper.

Throughout this derivation, we assume that different pixels $\mathbf{v}$ in a speckle pattern $u^{\mathbf{i}^n}(\mathbf{v})$ arising from one source are independent random variables. In practice, depending on magnification, the grain of speckle features on the sensor may be wider than a single pixel. This would imply some scaling adjustments in the exact formulas, which we neglect here. We also ignore small dependencies introduced by the low pass filtering of Eq. (4) and treat entries of $\bar{S}^{\mathbf{i}^n}(\mathbf{v})$ as independent random variables.

Also, in the following derivations expectations are taken with respect to multiple realization of scattering volumes with the same material parameters. For example, the notation $\mathbb{E}\left[\mathcal{C}^{I_1}(\mathbf{\Delta})\right]$ refers to the following. Suppose we had N different tissue layers of the same type, and we place behind each layer fluorescent sources at the exact same layout. We image N different speckle images and compute N different auto-correlations $\mathcal{C}^{I_1}(\mathbf{\Delta})$. For large N values averaging these auto-correlations provides the idealized expected speckle-auto correlation for that source layout, denoted $\mathbb{E}\left[\mathcal{C}^{I_1}(\mathbf{\Delta})\right]$. Similarly $\mathrm{Var}\left[\mathcal{C}^{I_1}(\mathbf{\Delta})\right]$ denotes the variance we expect to see in such auto-correlation. As correlation is computed from a finite number of speckle pixels the correlation is never zero even in displacements $\mathbf{\Delta}$ that do not correspond to an actual illuminator displacement. To define variance mathematically one needs to compute such auto-correlations from N different speckle images of the same illuminator layout. In practice for the evaluation in Fig. 8 we only compute the expectation and variance between different $\mathbf{\Delta}$ displacements of the auto-correlation of a single tissue sample.

Claim 1 *We define correlation contrast*

$$\Theta\left(\mathcal{C}^{I_1,\ldots,I_T}\right)=\frac{\frac{1}{|\Gamma_\Delta|}\sum_{\mathbf{\Delta}\in\Gamma_\Delta}\mathbb{E}\left[\mathcal{C}^{I_1,\ldots,I_T}(\mathbf{\Delta})\right]^2}{\frac{1}{|\Gamma_\Delta^c|}\sum_{\mathbf{\Delta}\in\Gamma_\Delta^c}\mathrm{Var}\left[\mathcal{C}^{I_1,\ldots,I_T}(\mathbf{\Delta})\right]} \tag{S1}$$

If the speckle patterns $S_t^{\mathbf{0}}$ are uncorrelated with each other for different t values, then the correlation contrast increases linearly *with the number of measurements T.*

Proof: The claim is based on the observation that for displacements $\mathbf{\Delta}\in\Gamma_\Delta$ that correspond to an actual illuminator's displacement, $\mathbb{E}\left[\mathcal{C}^{I_1,\ldots,I_T}(\mathbf{\Delta})\right]$ is a positive quantity, while for $\mathbf{\Delta}\in\Gamma_\Delta^c$, which do not correspond to a displacement between two illuminators, no correlation exists and in expectation $\mathbb{E}\left[\mathcal{C}^{I_1,\ldots,I_T}(\mathbf{\Delta})\right]=0$.

With this understanding, we note that expectation is linear and hence recalling the definition of $\mathcal{C}^{I_1,\ldots,I_T}(\mathbf{\Delta})$ in Eq. (10) of the main paper, the numerator of Eq. (S1) is independent of the number of measurements T:

$$\mathbb{E}\left[\mathcal{C}^{I_1,\ldots,I_T}(\mathbf{\Delta})\right]=\frac{1}{T}\sum_t\mathbb{E}\left[\mathcal{C}^{I_t}(\mathbf{\Delta})\right]=\mathbb{E}\left[\mathcal{C}^{I_1}(\mathbf{\Delta})\right]. \tag{S2}$$

We now move to express the denominator. First, we note that as our signal $I_1,\ldots,I_T$ are zero mean as defined in Eq. (14).

$$\mathrm{Var}\left[\mathcal{C}^{I_1,\ldots,I_T}(\mathbf{\Delta})\right]=\mathbb{E}\left[\left|\mathcal{C}^{I_1,\ldots,I_T}(\mathbf{\Delta})\right|^2\right] \tag{S3}$$

Thus, we expand the second moment below. Using again the definition of the average correlation in Eq. (10) of the main paper, we express:

$$\mathbb{E}\left[|\mathcal{C}^{I_1,\ldots,I_T}(\mathbf{\Delta})|^2\right]=\frac{1}{T^2}\sum_{(t_1,t_2)}\mathbb{E}\left[\mathcal{C}^{I_{t_1}}(\mathbf{\Delta})\cdot\mathcal{C}^{I_{t_2}}(\mathbf{\Delta})^*\right] \tag{S4}$$

$$=\frac{1}{T^2}\sum_t\mathbb{E}\left[\mathcal{C}^{I_t}(\mathbf{\Delta})\cdot\mathcal{C}^{I_t}(\mathbf{\Delta})^*\right] \tag{S5}$$

$$+\frac{1}{T^2}\sum_{(t_1\neq t_2)}\mathbb{E}\left[\mathcal{C}^{I_{t_1}}(\mathbf{\Delta})\right]\cdot\mathbb{E}\left[\mathcal{C}^{I_{t_2}}(\mathbf{\Delta})\right]^* \tag{S6}$$

$$=\frac{1}{T^2}\sum_t\mathbb{E}\left[|\mathcal{C}^{I_t}(\mathbf{\Delta})|^2\right] \tag{S7}$$

$$=\frac{1}{T}\mathbb{E}\left[|\mathcal{C}^{I_1}(\mathbf{\Delta})|^2\right] \tag{S8}$$

where Eq. (S6) follows from the assumption that for $t_1\neq t_2$ the speckles $S_{t_1}^{\mathbf{0}}, S_{t_2}^{\mathbf{0}}$ are uncorrelated with each other, and Eq. (S7) from the fact that for displacements $\mathbf{\Delta}\in\Gamma_\Delta^c$ the correlation has zero expectation.

From Eq. (S8), we conclude that as we increase the number of measurements the denominator scales as $1/T$. As a result the correlation contrast in Eq. (S1) scales linearly with T. ■

Below, we show that unlike the random modulation of Eq. (12), the LSI measurements of Eq. (13) do not reduce the correlation.

Claim 2 *For displacements in the order of a few speckle grains, the correlation between LSI signals $S_t^{\mathbf{i}^1}, S_t^{\mathbf{i}^2}$ produced by different illuminators $\mathbf{i}^1,\mathbf{i}^2$ is approximately the same as the correlation of the original speckle intensity images.*

Proof: As we filter the intensity images to have zero mean, the expected correlation becomes the *intensity covariance* C_I defined in [1]:

$$C_I\left(\left|u^{\mathbf{i}^1}(\mathbf{v})\right|^2,\left|u^{\mathbf{i}^2}(\mathbf{v}+\mathbf{\Delta})\right|^2\right) \tag{S9}$$

$$\equiv\mathbb{E}\left[|u^{\mathbf{i}^1}(\mathbf{v})|^2|u^{\mathbf{i}^2}(\mathbf{v}+\mathbf{\Delta})|^2\right]-\mathbb{E}\left[|u^{\mathbf{i}^1}(\mathbf{v})|^2\right]\mathbb{E}\left[|u^{\mathbf{i}^2}(\mathbf{v}+\mathbf{\Delta})|^2\right] \tag{S10}$$

Where the expectation is taken over multiple tissue layers of the same type. Classical statistics results state that the covariance between intensities is the square of the covariance between the complex zero mean fields u. Thus, the above definition can be further simplified to:

$$C_I\left(\left|u^{\mathbf{i}^1}(\mathbf{v})\right|^2,\left|u^{\mathbf{i}^2}(\mathbf{v}+\mathbf{\Delta})\right|^2\right)=\left|\mathbb{E}\left[u^{\mathbf{i}^1}(\mathbf{v})u^{\mathbf{i}^2}(\mathbf{v}+\mathbf{\Delta})^*\right]\right|^2 \tag{S11}$$

On the other hand, we consider the correlation between LSI signals:

$$C_I(S_t^{\mathbf{i}^1}(\mathbf{v}), S_t^{\mathbf{i}^2}(\mathbf{v}+\boldsymbol{\Delta})) \tag{S12}$$

$$= \mathbb{E}\left[S_t^{\mathbf{i}^1}(\mathbf{v}) S_t^{\mathbf{i}^2}(\mathbf{v}+\boldsymbol{\Delta})\right] - \mathbb{E}\left[S_t^{\mathbf{i}^1}(\mathbf{v})\right]\mathbb{E}\left[S_t^{\mathbf{i}^2}(\mathbf{v}+\boldsymbol{\Delta})\right] \tag{S13}$$

As before, the second term vanishes as in LSI, $S_t^{i^n}(\mathbf{v})$ is a zero mean signal. Also as we assume that different pixels of a speckle pattern are independent, we can express:

$$\mathbb{E}\left[S_t^{\mathbf{i}^1}(\mathbf{v}) S_t^{\mathbf{i}^2}(\mathbf{v}+\boldsymbol{\Delta})\right] \tag{S14}$$

$$= \mathbb{E}\left[u^{\mathbf{i}^1}(\mathbf{v}) u^{\mathbf{i}^1}(\mathbf{v}+\mathbf{d}_t)^* u^{\mathbf{i}^2}(\mathbf{v}+\boldsymbol{\Delta})^* u^{\mathbf{i}^2}(\mathbf{v}+\boldsymbol{\Delta}+\mathbf{d}_t)\right] \tag{S15}$$

$$= \mathbb{E}\left[u^{\mathbf{i}^1}(\mathbf{v}) u^{\mathbf{i}^2}(\mathbf{v}+\boldsymbol{\Delta})^*\right]\mathbb{E}\left[u^{\mathbf{i}^1}(\mathbf{v}+\mathbf{d}_t) u^{\mathbf{i}^2}(\mathbf{v}+\boldsymbol{\Delta}+\mathbf{d}_t)^*\right]^*.$$

Now we assume the displacement $\mathbf{d}_t$ is modest enough so that the correlation at pixel $\mathbf{v}$ and the correlation at a small displacement, at pixel $\mathbf{v}+\mathbf{d}_t$ is similar, so that

$$\mathbb{E}\left[u^{\mathbf{i}^1}(\mathbf{v}) u^{\mathbf{i}^2}(\mathbf{v}+\boldsymbol{\Delta})^*\right] \approx \mathbb{E}\left[u^{\mathbf{i}^1}(\mathbf{v}+\mathbf{d}_t) u^{\mathbf{i}^2}(\mathbf{v}+\boldsymbol{\Delta}+\mathbf{d}_t)^*\right]. \tag{S16}$$

Put all together, we can derive

$$C_I(S_t^{\mathbf{i}^1}(\mathbf{v}), S_t^{\mathbf{i}^2}(\mathbf{v}+\boldsymbol{\Delta})) \approx \left|\mathbb{E}\left[u^{\mathbf{i}^1}(\mathbf{v}) u^{\mathbf{i}^2}(\mathbf{v}+\boldsymbol{\Delta})^*\right]\right|^2 \tag{S17}$$

$$= C_I(\left|u^{\mathbf{i}^1}(\mathbf{v})\right|^2, \left|u^{\mathbf{i}^2}(\mathbf{v}+\boldsymbol{\Delta})\right|^2) \tag{S18}$$

■

We now show that despite the fact that we capture multiple images through the same tissue layer and our measurements are not independent, they are still uncorrelated which is enough to reduce the noise of the speckle auto-correlation we evaluate.

Claim 3 *For displacements $\mathbf{d}_{t_1}, \mathbf{d}_{t_2}$ whose distance $\|\mathbf{d}_{t_1} - \mathbf{d}_{t_2}\|$ is larger than the speckle grain, the signals $S_{t_1}^{i^n}, S_{t_2}^{i^n}$ are uncorrelated, so that*

$$\mathbb{E}\left[S_{t_1}^{i^n} \cdot S_{t_2}^{i^n *}\right] - \mathbb{E}\left[S_{t_1}^{i^n}\right] \cdot \mathbb{E}\left[S_{t_2}^{i^n}\right]^* = 0 \tag{S19}$$

Proof: Our derivation is based on the assumption that the speckle fields $u^{\mathbf{i}^n}$ have zero mean, and the speckle values in different sensor positions $\mathbf{v}$ are independent random variables. For a non zero displacement $\mathbf{d}_t$ we get

$$\mathbb{E}\left[S_t^{\mathbf{i}^n}\right] = \mathbb{E}\left[u^{\mathbf{i}^n}(\mathbf{v}) u^{\mathbf{i}^n}(\mathbf{v}+\mathbf{d}_t)\right]$$

$$= \mathbb{E}\left[u^{\mathbf{i}^n}(\mathbf{v})\right]\mathbb{E}\left[u^{\mathbf{i}^n}(\mathbf{v}+\mathbf{d}_t)\right] = 0. \tag{S20}$$

In a similar way

$$\mathbb{E}\left[S_{t_1}^{\mathbf{i}^n} S_{t_2}^{\mathbf{i}^n *}\right] = \mathbb{E}\left[u^{\mathbf{i}^n}(\mathbf{v}) u^{\mathbf{i}^n}(\mathbf{v}+\mathbf{d}_{t_1})^* u^{\mathbf{i}^n}(\mathbf{v})^* u^{\mathbf{i}^n}(\mathbf{v}+\mathbf{d}_{t_2})\right] \tag{S21}$$

$$= \mathbb{E}\left[|u^{\mathbf{i}^n}(\mathbf{v})|^2 u^{\mathbf{i}^n}(\mathbf{v}+\mathbf{d}_{t_1})^* u^{\mathbf{i}^n}(\mathbf{v}+\mathbf{d}_{t_2})\right] \tag{S22}$$

$$= \mathbb{E}\left[|u^{\mathbf{i}^n}(\mathbf{v})|^2\right]\mathbb{E}\left[u^{\mathbf{i}^n}(\mathbf{v}+\mathbf{d}_{t_1})\right]^*\mathbb{E}\left[u^{\mathbf{i}^n}(\mathbf{v}+\mathbf{d}_{t_2})\right] \tag{S23}$$

$$= 0. \tag{S24}$$

Where Eq. (S23) follows again from the assumption that speckle at different pixel positions are independent. Eq. (S20) and Eq. (S24) prove the desired Eq. (S19). ■

We now move to study the relationship between the correlation we can measure from LSI to the actual correlation of the latent pattern.

Claim 4 *For speckle fields $u^{\mathbf{i}^1}(\mathbf{v}), u^{\mathbf{i}^2}(\mathbf{v})$ satisfying the tilt shift relationship of Eq. (1), the LSI measurements $S_t^{\mathbf{i}^1}(\mathbf{v})$ and $S_t^{\mathbf{i}^2}(\mathbf{v})$ defined in Eq. (13) are shifted versions of each other, times a* globally constant *phasor, which is independent of pixel position $\mathbf{v}$. This is expressed by the relationship:*

$$S_t^{\mathbf{i}^1}(\mathbf{v}) \approx S_t^{\mathbf{i}^2}(\mathbf{v}+\boldsymbol{\Delta}) e^{-jk\alpha(\mathbf{d}_t{}^T\boldsymbol{\Delta})}, \tag{S25}$$

with $\boldsymbol{\Delta} = \mathbf{i}^2 - \mathbf{i}^1$.

Proof: From Eq. (1), we have $u^{\mathbf{i}^1}(\mathbf{v}) \approx e^{jk\alpha(\boldsymbol{\tau}^T\boldsymbol{\Delta})} u^{\mathbf{i}^2}(\mathbf{v}+\boldsymbol{\Delta})$, with $\boldsymbol{\tau} = \mathbf{v} - \mathbf{i}^1$. Substituting into Eq. (13) we have,

$$\begin{aligned} S_t^{\mathbf{i}^1}(\mathbf{v}) &= u^{\mathbf{i}^1}(\mathbf{v}) u^{\mathbf{i}^1}(\mathbf{v}+\mathbf{d}_t)^* \\ &\approx e^{jk\alpha(\boldsymbol{\tau}^T\boldsymbol{\Delta})} u^{\mathbf{i}^2}(\mathbf{v}+\boldsymbol{\Delta}) e^{-jk\alpha<\boldsymbol{\Delta},\boldsymbol{\tau}+\mathbf{d}_t>} u^{\mathbf{i}^2}(\mathbf{v}+\boldsymbol{\Delta}+\mathbf{d}_t)^* \\ &= e^{-jk\alpha(\mathbf{d}_t{}^T\boldsymbol{\Delta})} u^{\mathbf{i}^2}(\mathbf{v}+\boldsymbol{\Delta}) u^{\mathbf{i}^2}(\mathbf{v}+\boldsymbol{\Delta}+\mathbf{d}_t)^* \\ &= e^{-jk\alpha(\mathbf{d}_t{}^T\boldsymbol{\Delta})} S_t^{\mathbf{i}^2}(\mathbf{v}+\boldsymbol{\Delta}) \end{aligned}$$

■

With all the above claims we are now ready to prove our main result and show that the global phasor of the previous claim translates into a phase ramp in the auto-correlation.

Claim 5 *Using the LSI measurements of Eq. (13), the speckle auto-correlation $\mathcal{C}^{I_t} = I_t \star I_t$ is equivalent to the auto-correlation of the latent pattern $\mathcal{C}^O = O \star O$, times a phase ramp correction*

$$\mathcal{C}^{I_t}(\boldsymbol{\Delta}) \approx \mathcal{C}^O(\boldsymbol{\Delta}) e^{-jk\alpha(\mathbf{d}_t{}^T\boldsymbol{\Delta})}. \tag{S26}$$

Proof: Using Claim 4 for the specific case $\mathbf{i}^1 = \mathbf{i}^n$ and $\mathbf{i}^2 = \mathbf{0}$ we get $S_t^{i^n}(\mathbf{v}) \approx S_t^{\mathbf{0}}(\mathbf{v}+\mathbf{i}^n) e^{-jk\alpha(\mathbf{d}_t{}^T\mathbf{i}^n)}$. Summing over all sources $S_t^{i^n}(\mathbf{v})$ we have

$$I_t(\mathbf{v}) \approx S_t^{\mathbf{0}} * \tilde{O}.$$

with $\tilde{O}$

$$\tilde{O}(\mathbf{v}) = O(\mathbf{v}) e^{-jk\alpha(\mathbf{d}_t{}^T\mathbf{v})}. \tag{S27}$$

This is due to the fact that O is non zero only at positions $\mathbf{v} = \mathbf{i}^n$ for one of the sources, so effectively $\tilde{O}$ has for each sensor position $\mathbf{i}^n$ the global phasor of Eq. (S25). As in the standard derivation of the speckle auto-correlation we assume $S_t^{\mathbf{0}} \star S_t^{\mathbf{0}} = \delta$, and hence

$$I_t \star I_t \approx \tilde{O} \star \tilde{O}. \tag{S28}$$

or equivalently

$$\mathcal{C}^{I_t}(\boldsymbol{\Delta}) \approx \mathcal{C}^{\tilde{O}}(\boldsymbol{\Delta}). \tag{S29}$$

Hence we are left with the need of computing $\mathcal{C}^{\tilde{O}}(\boldsymbol{\Delta})$. We note that by the Wiener-Khinchin theorem, $\mathcal{C}^{\tilde{O}}(\boldsymbol{\Delta})$ is the inverse Fourier transform of $\left|\mathcal{F}(\tilde{O})\right|^2$. However as $\tilde{O}$ is obtained by multiplying O with a phase ramp (see Eq. (S27)), their Fourier transforms are related via a shift:

$$\mathcal{F}(\tilde{O})(\boldsymbol{\omega}) = \mathcal{F}(O)(\boldsymbol{\omega} + \alpha\mathbf{d}_t). \tag{S30}$$

The shift relation holds also for their absolute values

$$\left|\mathcal{F}(\tilde{O})(\boldsymbol{\omega})\right|^2 = \left|\mathcal{F}(O)(\boldsymbol{\omega} + \alpha\mathbf{d}_t)\right|^2 \tag{S31}$$

Hence $\mathcal{C}^{\tilde{O}}(\boldsymbol{\Delta})$ and $\mathcal{C}^O(\boldsymbol{\Delta})$ are related via a tilt:

$$\mathcal{C}^{\tilde{O}}(\boldsymbol{\Delta}) = \mathcal{C}^O(\boldsymbol{\Delta}) e^{-jk\alpha(\mathbf{d}_t{}^T\boldsymbol{\Delta})}. \tag{S32}$$

Substituting Eq. (S32) in Eq. (S29) proves the desired Eq. (S26).

■

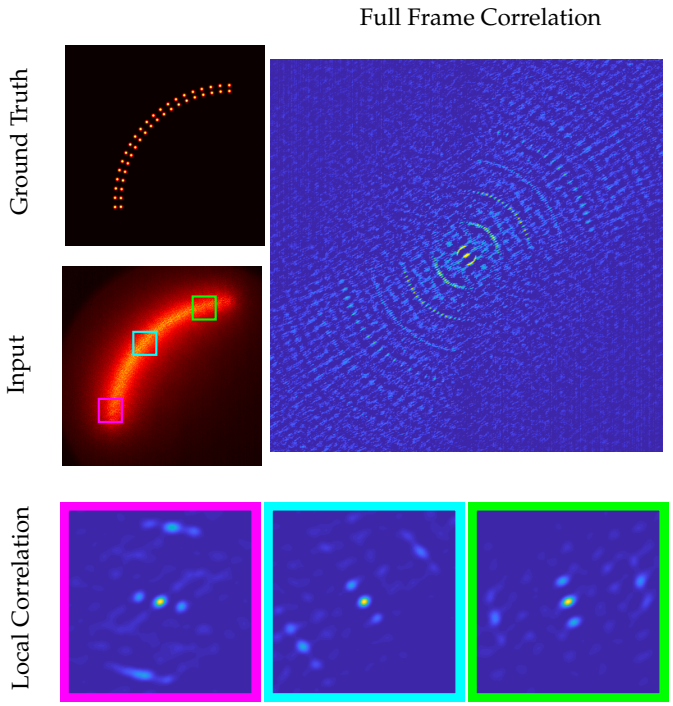

Fig. S1. Local versus global auto-correlation. The orientation of the auto-correlation evaluated in three different local windows of the image matches the orientation of the arc in the corresponding region of the latent image. By contrast, the auto-correlation of the full frame is much nosier, and decays for large displacements due to limited ME.

B. OPTIMIZING USING LOCAL SUPPORT

For sources located inside the scattering medium, speckle patterns emerging from a single source have local support and do not spread over the entire sensor. To take advantage of this property, [1] suggest matching the local speckle correlations in the image, rather than the full-frame auto-correlation. We review this algorithm below.

For motivation, consider Fig. S1 that we re-plot from [1]. It visualizes speckles produced by latent incoherent illuminators in a double arc layout. Computing auto-correlation at small subwindows of the speckle image reveals the local orientation of the arc in the latent image. By contrast, when computing the auto-correlation of the full frame, the correlation is considerably noisier even for small displacements. Correlations between far illuminators are even harder to detect due to the fact that the ME range is limited and for large displacements $\mathbf{\Delta}$ the desired correlation (see Eq. (1)) is very weak.

The optimization algorithm takes as input two threshold parameters T_τ, T_Δ. It assumes that speckles from one illuminator are spread over pixels in a window of size T_τ around it, and that ME correlation holds for displacements $|\mathbf{\Delta}| < T_\Delta/2$. The thresholds T_τ, T_Δ are free parameters that can be fine-tuned to improve reconstruction quality, and [1] show that performance are not too sensitive to their exact values. In all of our experiments, we fixed $T_\tau = 8\mu m$ and $T_\Delta = 48\mu m$.

The algorithm offers improved performance compared to the baseline full-frame auto-correlation algorithm in situations where $T_\tau < T_\Delta$, namely when the support from one illuminator is lower than the ME range. For thick scattering slices, where high-order scattering is dominant, this relationship does not hold and the approach reduces to the baseline full-frame auto-correlation algorithm.

The algorithm searches for a latent image O such that the auto-correlation in its local windows will match the auto-correlation in the local windows of the input image I. We define $w^{\mathbf{\Delta}}$ and $w^{\boldsymbol{\tau}}$ to be binary windows with support T_Δ, T_τ, respectively, and $\bar{w}^{2\boldsymbol{\tau}} = w^{\boldsymbol{\tau}} \star w^{\boldsymbol{\tau}}$—note that, from its definition, $\bar{w}^{2\boldsymbol{\tau}}$ is non-binary. Then, we recover O by solving the optimization problem:

$$\min_{O} \sum_p \| \frac{1}{T} \sum_t e^{jk\alpha({\mathbf{d}_t}^T \mathbf{\Delta})} \cdot I_{t,w_p^{\boldsymbol{\tau}}} \star I_{t,w_p^{\mathbf{\Delta}}} - O_{\bar{w}_p^{2\boldsymbol{\tau}}} \star O_{w_p^{\mathbf{\Delta}}} \|^2, \quad \textbf{(S33)}$$

where $I_{t,w_p^{\boldsymbol{\tau}}}, I_{t,w_p^{\mathbf{\Delta}}}, O_{\bar{w}_p^{2\boldsymbol{\tau}}}, O_{w_p^{\mathbf{\Delta}}}$ denote windows of a given size cropped from the input and latent images, centered around the p-th pixel.

Eq. (S33) uses windows of three different sizes, and we use Fig. S2 to visualize their different roles: Each $w_p^{\boldsymbol{\tau}}$ is a small window around pixel p whose support is equivalent to the expected support size of the speckle pattern due to a single illuminator. $w_p^{\mathbf{\Delta}}$ is a larger window around the same pixel, corresponding to the maximal displacement T_Δ for which we expect to find correlation, as dictated by the ME range.

We note, additionally, that the window cropped from O should be wider than that from I. This is because speckle at a certain pixel can arise from an illuminator within a window around it. For example, in Fig. S2, no illuminator is located inside the cyan subwindow of O, but part of the speckle pattern of a neighboring source is leaking into the corresponding cyan subwindow of I. As a result $O_{w_p^{\boldsymbol{\tau}}} \star O_{w_p^{\mathbf{\Delta}}}$ is a zero image, even though $I_{w_p^{\boldsymbol{\tau}}} \star I_{w_p^{\mathbf{\Delta}}}$ detects three impulses. It is easy to prove that this can be addressed using the larger, non-binary window $\bar{w}^{2\boldsymbol{\tau}}$ in the latent image, indicated in Fig. S2 using dashed lines: in this case, $O_{\bar{w}_p^{2\boldsymbol{\tau}}} \star O_{w_p^{\mathbf{\Delta}}}$ correctly detects the same three impulses as $I_{w_p^{\boldsymbol{\tau}}} \star I_{w_p^{\mathbf{\Delta}}}$.

The motivation for the cost of Eq. (S33) is that, even if two illuminators in the latent pattern O are at a distance larger than the ME range T_Δ, they can be recovered if there exists a sequence of illuminators between them, where each two consecutive illuminators in the sequence are separated by a distance smaller than T_Δ. For example, in Fig. S2, the illuminators outside the yellow and cyan $w^{\mathbf{\Delta}}$ windows are recovered thanks to the intermediate illuminators.

The optimization problem in Eq. (S33) is no longer a phase retrieval problem as in standard full-frame auto-correlation algorithms. We minimize it using the ADAM gradient-based optimizer [2]. Gradient evaluation is described in [1], and reduces to a sequence of convolution operations that can be performed efficiently, e.g., using a GPU based fast Fourier transform. For initialization, we set the latent image to random noise; we have observed empirically that the optimization is fairly insensitive to initialization. Finally, we note that even though we could place a window w_p around every pixel of I, the empirical correlation is insensitive to small displacements of the central pixel p. Therefore, in practice, we consider windows only at strides $T_\tau/2$, which helps reduce computational complexity.

We note that the optimization problem of Eq. (S33) is similar to ptychography algorithms [3]. However, we emphasize that previous ptychographic approaches for extending the ME range recover the latent illuminators from *multiple* image measurements, captured by sequentially exciting different areas on the scattering sample [4–8]. By contrast, our algorithm recovers the latent illuminators from a fixed number of full-frame shots.

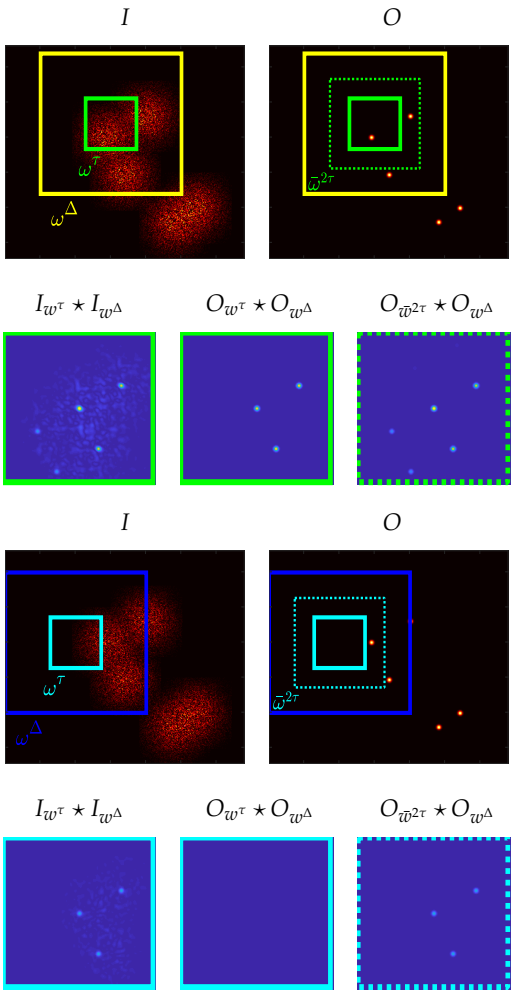

Fig. S2. Local window selection for optimization. We consider local subwindows w^τ (light green and cyan frames) whose support is equivalent to the speckle support size. Each such window is correlated with a wider window w^Δ (yellow and blue frames) around it, whose support is equivalent to the ME range. As speckle inside window w^τ can arise from a source outside w^τ, $O_{w^\tau} \star O_{w^\Delta}$ may not match $I_{w^\tau} \star I_{w^\Delta}$. To overcome this, we use an extended non-binary sub-window $\bar{w}^{2\tau} = w^\tau \star w^\tau$ for O, whose support is indicated by dashed lines.

C. LOCAL SUPPORT AND PSF AUTO-CORRELATION

As mentioned in Sec. 2.A, ME-based reconstruction algorithms are based on the assumption that the auto-correlation of a speckle pattern $\bar{S}^{\mathbf{0}}$ generated by a single source is an impulse, i.e. $\bar{S}^{\mathbf{0}} \star \bar{S}^{\mathbf{0}} \approx \delta$. When $\bar{S}^{\mathbf{0}}$ has a limited support, this is only an approximation and $\bar{S}^{\mathbf{0}} \star \bar{S}^{\mathbf{0}}$ is an impulse plus noise. In Fig. S3 we demonstrate the auto-correlation of speckle patterns with different supports. As the support increases, its auto-correlation better approximates a clean impulse.

D. CHOICE OF DISPLACEMENTS IN LSI

Our algorithm is not sensitive to the exact selection of LSI displacements, as demonstrated in Fig. S4. These displacements should only satisfy the following two properties. First the displacements need to be larger than the speckle grain, as set by the NA of the imaging system. Second the distance needs to be smaller than the support of the speckle pattern generated by a single source.

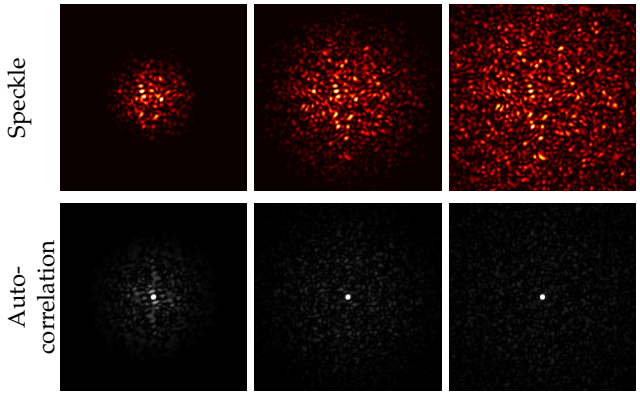

Fig. S3. Auto-correlation with different speckle support. Top row: We simulated speckle patterns with different supports. Lower row: The auto-correlation of the speckle pattern. With smaller support the auto-correlation involves a dominant noise component. As support increases the auto-correlation approaches an impulse.

In our implementation we used 18 $\mathbf{d}_t$ displacements visualized in Fig. S5. These span different directions and distances, where 6 of them are shifted by 1.6 um (5 pixels) with angles = $[0, \frac{\pi}{3}, ..., \frac{5\pi}{3}]$, and 12 of them are shifted by 3.3 um (10 pixels) with angles = $[0, \frac{\pi}{6}, ..., \frac{11\pi}{6}]$. Since each interferometric measurement requires 3 images, we take a total of 54 images.

E. HARDWARE PROTOTYPE AND ADDITIONAL RESULTS

We visualize the hardware schematic in Fig. 4 and its image in Fig. S6. Also, in Fig. S7 and Fig. S8 we show additional reconstruction results using fluorescent bead targets as well as translating laser targets. Both used tissue slices of thickness around ~150μm. In Fig. S14 we use fluorescent beads behind a parafilm phantom, see characterization in Sec. I.

F. PHASE CORRECTION IN LSI

As noted in Claim 4, when using our LSI, we need a phase ramp correction to the auto-correlation of speckles. To support the claim, we compare results with and without the correction. In Fig. S9, we show the auto-correlation obtained by averaging LSI measurements I_t (Eq. (14)) with and without the phase ramp correction of Eq. (16). The phase correction further improves the contrast, especially at larger displacements $\mathbf{\Delta}$. In Fig. S10 we further show the reconstruction result of LSI with and without the phase ramp correction. If the phase correction is not used the distance sources are not recovered.

The desired α value for Eq. (16) should match the α value of the ME correlation in Eq. (1), which was derived in [9] as $\alpha \approx \frac{-3}{2L}$. Our tissue is around 150um thick, but between tissue and beads, there is another cover slides also around 150um thick, so $L \approx 300\mu m$ and thus in principle we should use $\alpha \approx -0.005$. In practice we have manually adjusted the selection of α around this theoretical prediction to improve the visual quality

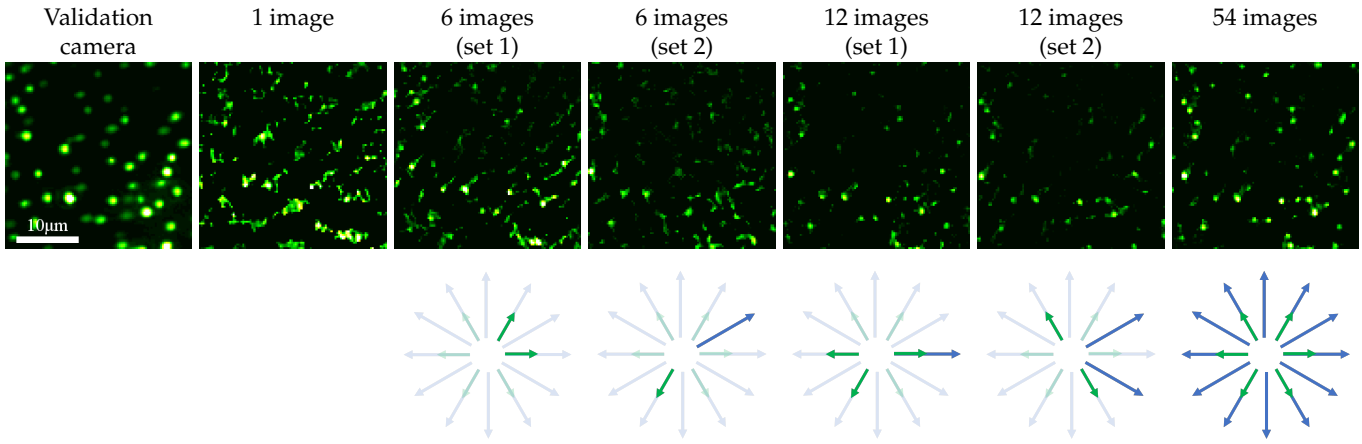

Fig. S4. Evaluating reconstruction vs. number of shots with different selections of the $\mathbf{d}_t$ values. Top part: we visualize again the reconstructions of Fig. 9. For g and 12 shots we demonstrate different selections of the $\mathbf{d}_t$ values in the 6 and 12 image results, leading to comparable reconstructions. Bottom part: visualization of the selected $\mathbf{d}_t$ values (each $\mathbf{d}_t$ shift is captured using 3 shots).

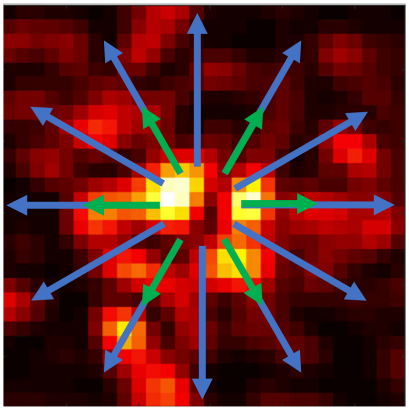

Fig. S5. $\mathbf{d}_t$ visualization. We demonstrate a typical speckle pattern and the set of 18 displacement $\mathbf{d}_t$ we used in our *LSI* implementation.

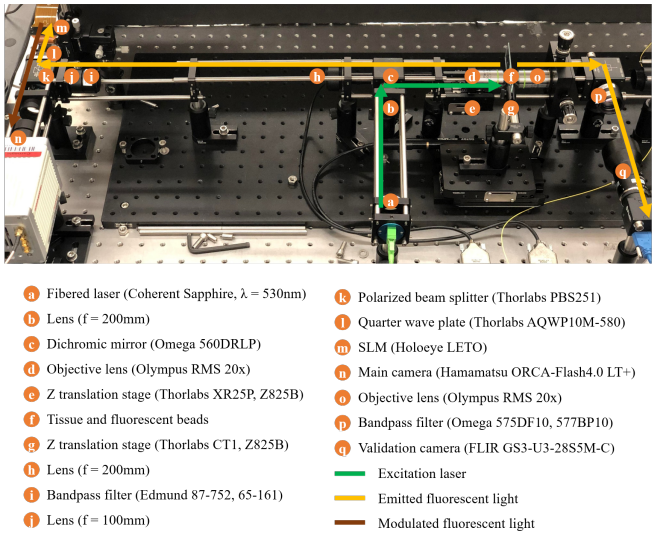

Fig. S6. Hardware prototype. Image of our prototype, analogous to the schematic in Fig. 4.

of the results and increase contrast. In Fig. S11 we visualize reconstructions for different α values. Results are not sensitive to the exact selection of this parameter, with multiple values leading to comparable results.

G. RECONSTRUCTION BEYOND THE ME RANGE

As explained by [1] the local correlation approach can recover objects whose extent is wider than the ME, because it only relies on local correlations and does not assume correlation between any two distant sources. While this was exhaustively demonstrated in their paper, we provide here one empirical evaluation of this property.

Since our scanning laser setup captures speckle patterns by different point sources separately, we can compute the correlation between speckle patterns generated by individual sources. We plot this correlation as a function of the displacement between the sources. In Fig. S12, we plot the correlation we evaluated on the data of Fig. 7. It can be seen that this correlation drops bellow 0.5 when the source distance is $10\mu m$. At the same time, the reconstructed pattern is 6 times wider, spanning a range of $60\mu m$, as in Fig. 7.

Furthermore, note that Fig. 1 reconstructs beads spread over a $300\mu m \times 300\mu m$ range. While we do not have ground truth correlations for this tissue sample, the samples in Fig. 1 and Fig. 7 have about the same thickness of $150\mu m$, hence we believe they have similar ME correlation ranges.

H. TISSUE THICKNESS

In Fig. S13 we used the scanning laser setup to create the same illumination layout behind different tissue slices. This allows us to compare reconstructions through different tissue thicknesses. For the thickest layer the reconstruction failed.

As discussed in [1], thicker tissue leads to larger speckle spread and weaker memory effect correlation. As we used the scanning laser setup we can again compute the ME correlation, plotted at the lower part of Fig. S13. As expected, as the tissue thickness increases the correlation decays faster as a function of displacement, explaining the reconstruction failure in the lowest

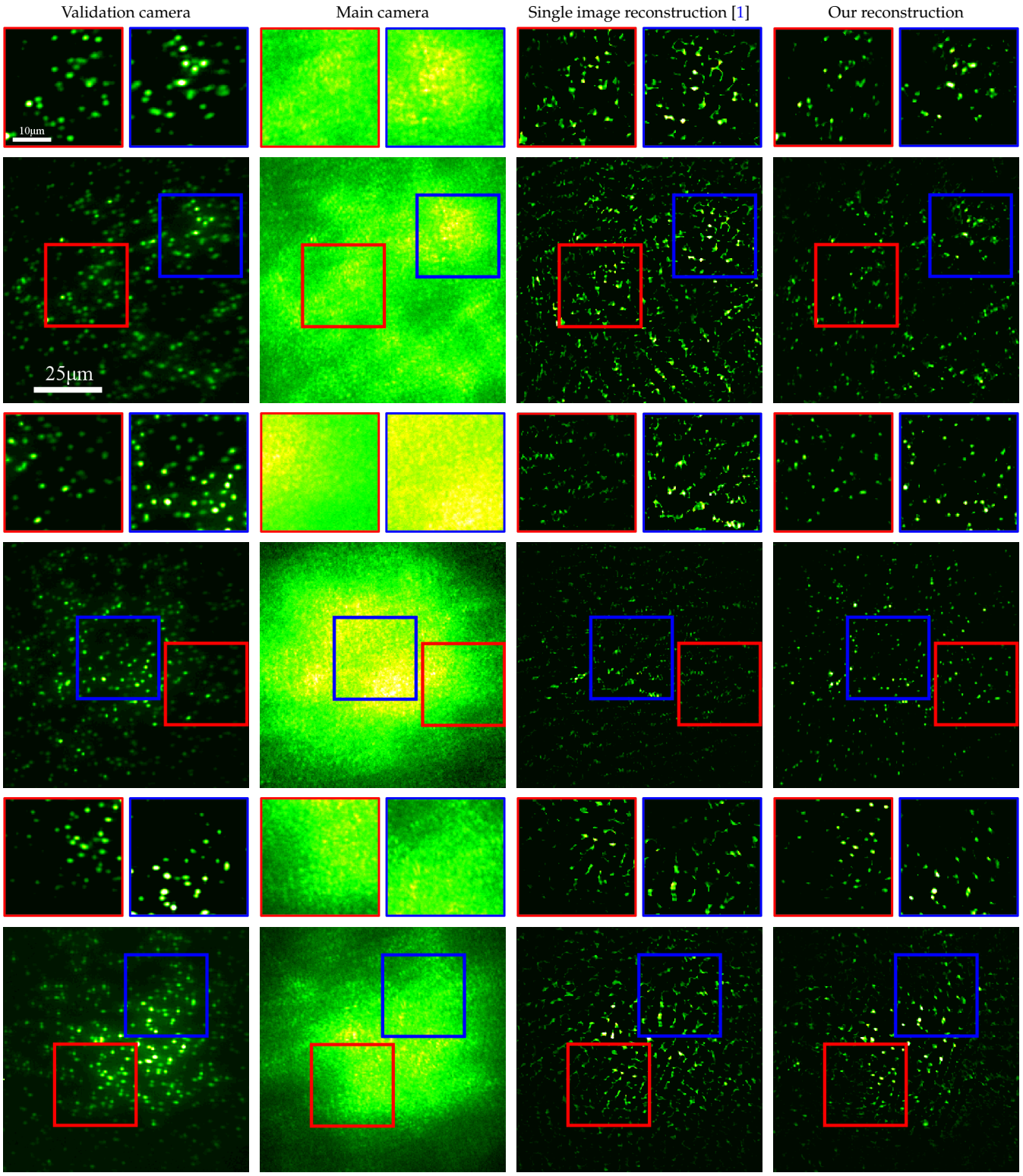

Fig. S7. Additional reconstruction results for fluorescent beads behind ~150μm-thick tissue slices. With LSI, we can clearly reconstruct fluorescent bead targets from 54 shot images captured by the main camera. The reconstruction is compared against a reference image from the validation camera observing the beads directly. In contrast, a standard single-image shot of the scattered light only facilitates a very noisy reconstruction.

row.

These results demonstrate the limitation of our method: while we can improve correlation contrast, our approach is still based on the existence of some memory effect correlation and will fail

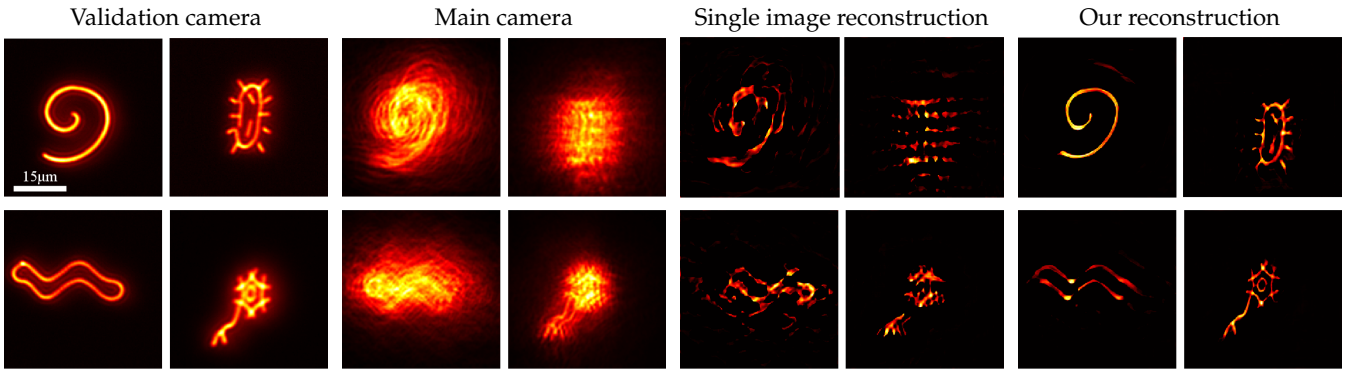

Fig. S8. Additional reconstruction results for inputs captured using the translating laser setup, behind ~150μm-thick tissue slices. With LSI, we can clearly reconstruct structured targets with different layouts, while a reconstruction from a single shot is noisier.

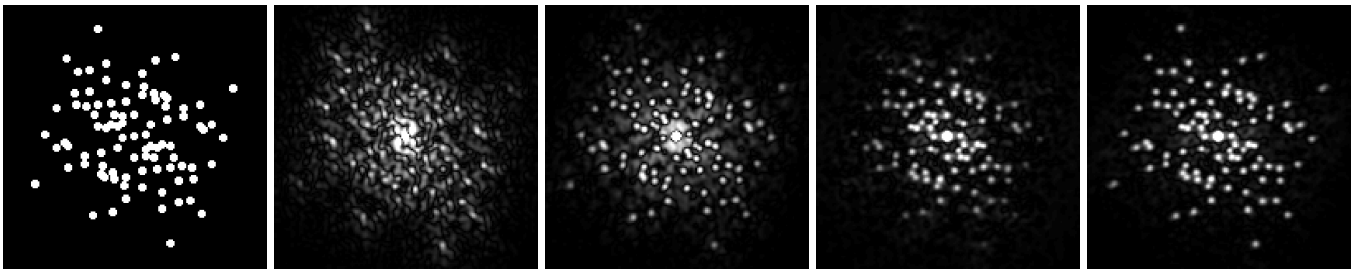

(a) Ground truth (b) No diversification [1] (c) Random modulation (d) LSI (phase uncorrected) (e) LSI

Fig. S9. Comparing speckle auto-correlation in LSI with and without phase correction. (a) Ground-truth auto-correlation. (b) Auto-correlation from a single speckle image with no diversification. (c) Random phase mask in the Fourier plane. (d) LSI auto-correlations without correction. The larger displacements at the outer image regions are degraded due to phase variations. (e) After phase correction, LSI auto-correlations can recover further displacements.

when this correlation is too weak.

I. TISSUE PREPARATION AND CHARACTERIZATION

Most results in this paper used chicken breast tissue as a scattering material. We cut thin slice from thawed chicken breast. To keep the tissue fresh, we did the fluorescent imaging experiment within 3 hours. The scanning laser targets require longer capture. To keep freshness we squeeze the tissue between two cover glasses and seal them using nail polish.

As stated in [10], chicken breast tissue has an anisotropy parameter $g = 0.965$ and a mean free path (MFP) around $43.7\mu m$. However, these parameters may vary significantly between different tissue slices.

For a better characterization, we also use a parafilm phantom. This was calibrated in [11], reporting an anisotropy parameter $g = 0.77$ and a MFP around $170\mu m$. We imaged through one parafilm layer whose thickness is about $120\mu m$. Results for this phantom are demonstrated in Fig. S14. Note that while the parafilm has a longer MFP, it also has a smaller anisotropy factor and in practice the speckle spreads of both parafilm and chicken breast are comparable.

REFERENCES

1. M. Alterman, C. Bar, I. Gkioulekas, and A. Levin, "Imaging with local speckle intensity correlations: theory and practice," ACM TOG (2021).
2. D. P. Kingma and J. Ba, "Adam: A method for stochastic optimization," ICLR (2015).
3. J. M. Rodenburg, A. C. Hurst, A. G. Cullis, B. R. Dobson, F. Pfeiffer, O. Bunk, C. David, K. Jefimovs, and I. Johnson, "Hard-x-ray lensless imaging of extended objects," Phys. Rev. Lett. **98** (2007).
4. M. Zhou, A. Pan, R. Li, Y. Liang, J. Min, T. Peng, C. Bai, and B. Yao, "Retrieval of non-sparse object through scattering media beyond the memory effect," J. Opt. (2020).
5. D. F. Gardner, S. Divitt, and A. T. Watnik, "Ptychographic imaging of incoherently illuminated extended objects using speckle correlations," Appl. Opt. (2019).
6. G. Li, Y. Wanqin, W. Haichao, and G. Situ, "Image transmission through scattering media using ptychographic iterative engine," Appl. Sci. (2019).
7. L. Li, X. Wen, R. Song, J.-T. Jiang, H.-L. Zhang, X.-B. Liu, and L. Wei, "Imaging correlography using ptychography," Appl. Sci. (2019).
8. N. Shekel and O. Katz, "Using fiber-bending-generated speckles for improved working distance and background rejection in lensless micro-endoscopy," Opt. Lett. **45**, 4288–4291 (2020).
9. G. Osnabrugge, R. Horstmeyer, I. N. Papadopoulos, B. Judkewitz, and I. M. Vellekoop, "Generalized optical memory effect," Optica (2017).
10. S. Schott, J. Bertolotti, J.-F. Léger, L. Bourdieu, and S. Gigan, "Characterization of the angular memory effect of scattered light in biological tissues," Opt. express **23**, 13505–13516 (2015).
11. A. Boniface, B. Blochet, J. Dong, and S. Gigan, "Noninvasive light focusing in scattering media using speckle variance optimization," Optica **6**, 1381–1385 (2019).

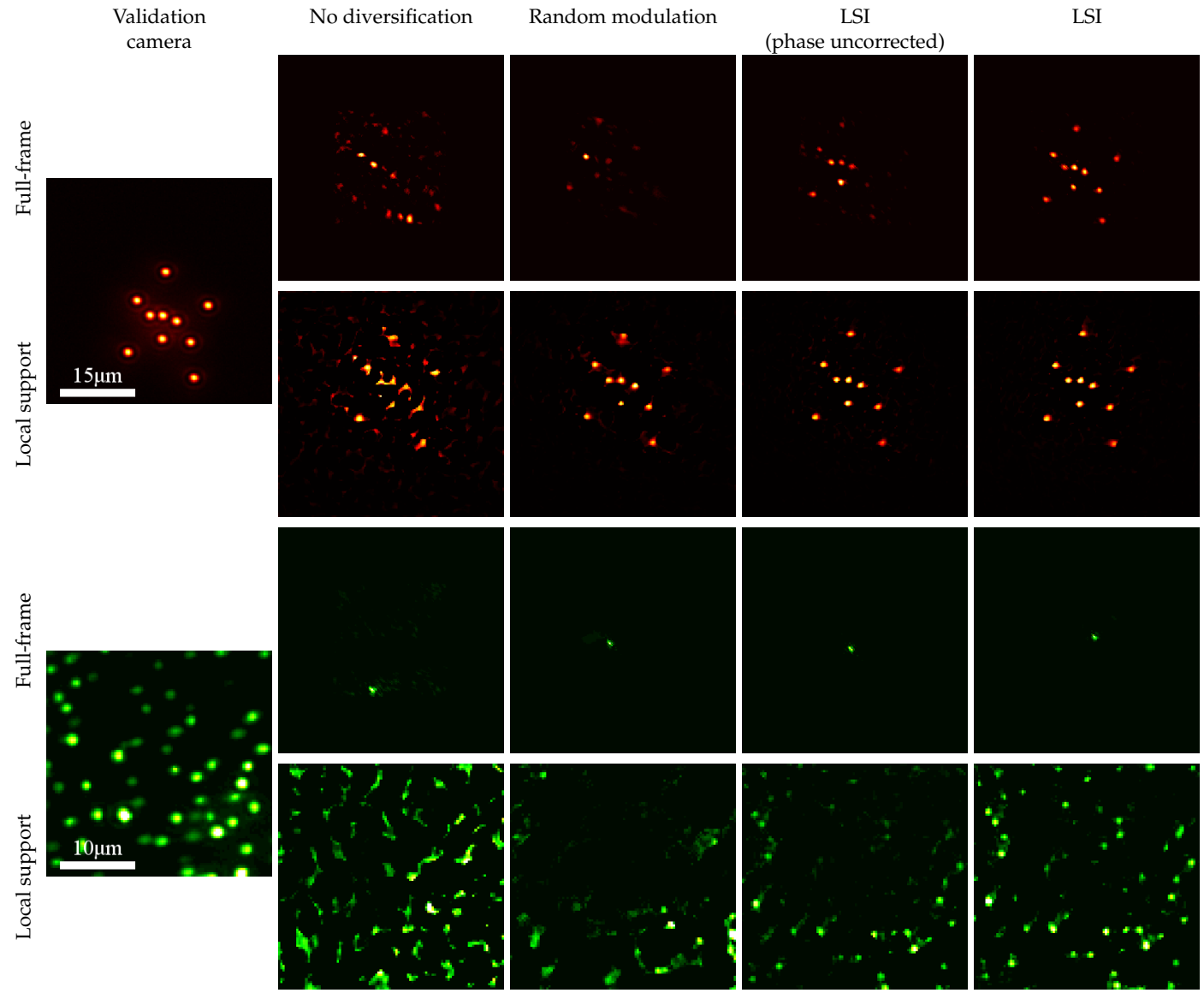

Fig. S10. Comparing LSI with and without phase correction. In addition to Fig. 6, we compare LSI without phase correction. Top part: sparse, simple shifting laser target. Lower part: challenging fluorescent beads target. For the simple target on the top, the full-frame algorithm using the auto-correlation of the LSI measurements without phase correction fails to recover the further beads. The local correlation approach which is more robust to noise can recover the target with and without correlation. For the challenging target at the lower part, the full-frame algorithm fails completely even with phase correction. The local correlations algorithm can reconstruct the target using LSI modulations. However, without phase correction, it can only reconstruct a subset of the beads.

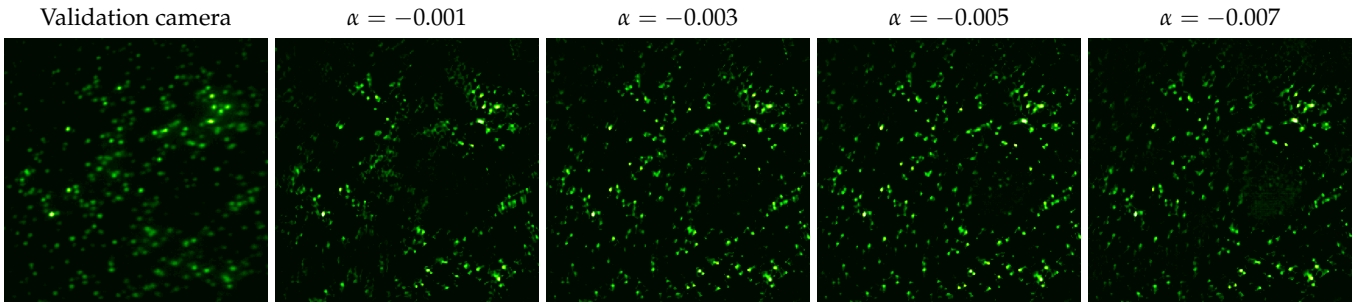

Fig. S11. Reconstruction with different α values in Eq.(16). In theory, $\alpha \approx -0.005$ in our setting, but comparable results are obtained with multiple α values.

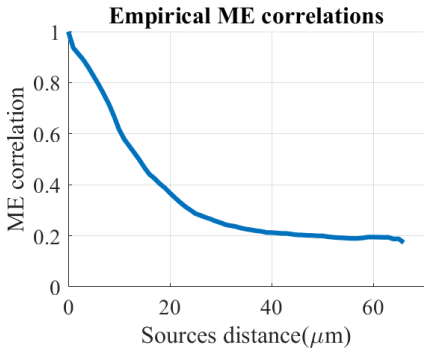

Fig. S12. Reconstruction beyond the ME range. As the shifting laser setup allows capturing speckles from individual sources independently, we can empirically compute the decay of speckle correlation as a function of the distance between the sources. We show such empirical correlation computed from the data in the bottom row of Fig. 7. While ME correlation decays below 0.5 for sources separated by as little as $10\mu m$, the reconstructed object is significantly wider than the ME range, spanning an area of $\sim 60\mu m \times 60\mu m$.

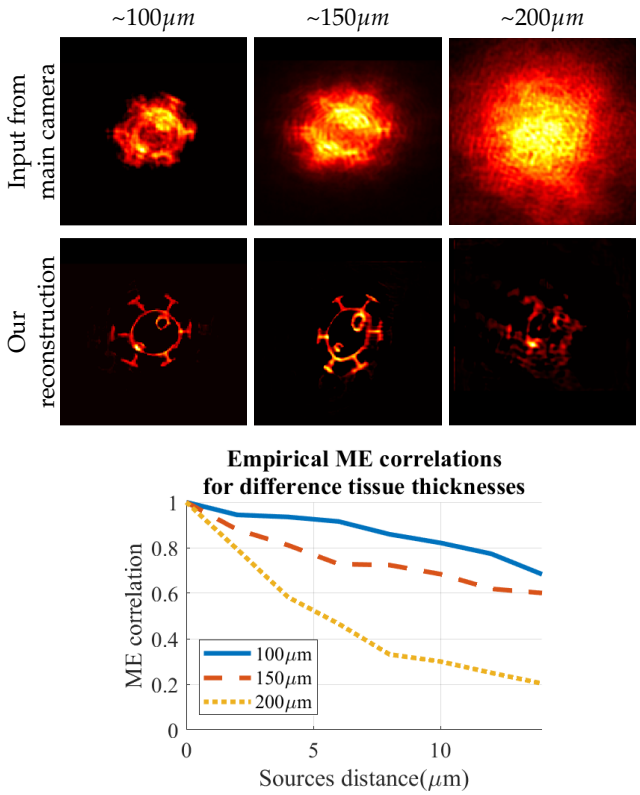

Fig. S13. Compare reconstructions with different tissue thickness. Top panel: We use the shifting laser acquisition to capture the same illumination pattern through three different tissue slices of increasing thicknesses. As tissue thickness increase the spread of the speckles is wider and the statistical correlations are weaker. With the ~$200\mu m$-thick tissue the correlations are too wreak and reconstruction fails. Lower panel: As the shifting laser setup allows capturing speckles from individual sources independently, we can empirically compute the decay of speckle correlation as a function of the distance between the sources. Indeed for thicker tissue slices the correlation decays faster as a function of source separation. This explains the reconstruction failure for the ~$200\mu m$-thick tissue example.

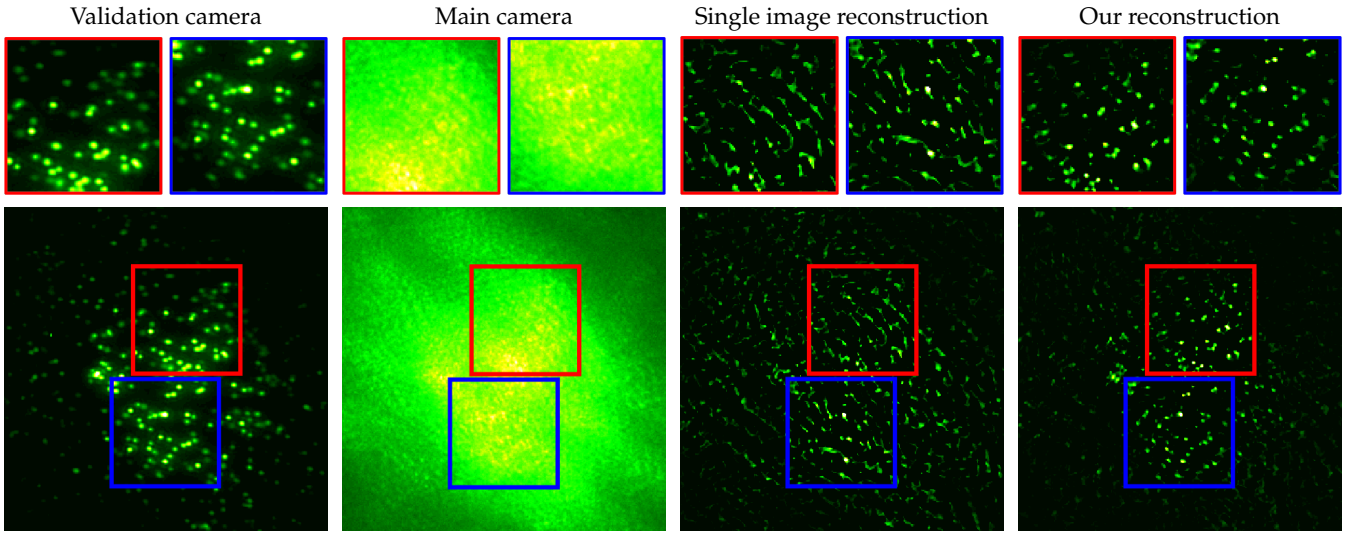

Fig. S14. Additional results. reconstructing fluorescent beads behind a parafilm phantom.